International Journal of Engineering Trends and Technology
ISSN: 2231 – 5381 / https://doi.org/10.14445/22315381/IJETT-V70I8P235

Volume 70 Issue 8, 336-346, August 2022

Original Article

Effect of Cosine Shape Stenosis on non-Newtonian Blood Flow with Casson Model in Stenosed Artery

Manisha[1], Surendra Kumar[2]

[1,2]*University Institute of Engineering and Technology, Maharishi Dayanand University, Haryana, India*

[1]manisharana88@gmail.com

Received: 06 June 2022 Revised: 04 August 2022 Accepted: 15 August 2022 Published: 27 August 2022

Abstract - *The objective of the manuscript is to find the effect of cosine shape stenosis on different physical properties such as skin friction, resistance to flow, and flow rate of the stenosed artery. The Casson fluid is a thin shear fluid at high viscosity, and blood can be considered an example of Casson fluid. Numerical computation for different flow quantities normalized with Newtonian and non-Newtonian fluid has been done with the help of the two-point Gauss quadrature formula. The normalized flow resistance with Newtonian fluid increases with stenosis depth. However, normalized flow resistance with non-Newtonian fluid reduces by enhancement of yield stress. The normalized skin friction with Newtonian fluid is increased by increasing the yield stress value; normalized skin friction with non-Newtonian fluid is highest at stenosis throat, and lowest at the artery ends.*

Keywords - *Newtonian fluid, Non-Newtonian fluid, Viscosity coefficient, Yield stress.*

1. Introduction

Atherosclerosis is one of the main health risks, and it refers to the contraction of the artery. It increases by some greasy substances or cholesterol-enriched lipid substances. This unnatural and abnormal expansion in the artery is called stenosis, which distracts the blood flow. The atherosclerotic plaque results in high flow resistance, pressure, and velocity variations. The geometry of the stenosis has a great influence on pressure, directions, and wall shear stress. The stenosis's physical properties, like shape and size, affect the flow behaviour through cylindrical arteries, as Lorenzini and Casalena [10]. The high strain in the artery is caused by stenosis, which has the geometry of trapezium plaque shape, resulting in more probability of artery blockage.

Many researchers have different opinions on blood characteristics inside the arteries, and blood is assumed as Newtonian fluid in manuscripts [9],[18]. In contrast, blood flow is considered a non-Newtonian fluid in manuscripts [11], [15]. The blood was demonstrated by the power-law fluid model in many manuscripts. Casson [4] also examined the validity of the Casson model for blood flow. Blair [2] and Copley [5] also examined the validity of the Casson model for blood flow. They found that Casson fluid model could demonstrate shear behaviour in narrow-sized blood arteries. Merrill et al. [12] reported that the Casson model having tubes of a diameter of 130-1000μm could be used for blood flow. Charm and Kurland [6] found that blood flow in slim arteries at a small shear rate could be demonstrated by Casson fluid model, and it could be used for large range shear rates and hematocrit. Blair and Spanner [3] also found that the blood flow model was demonstrated by the Casson model at a medium shear rate of blood. As per the theory of Aroesty and Gross [1], pulsating blood flow can be demonstrated by the Casson model when the flow is through narrow arteries. Chaturani and Samy [7] used the perturbation method to represent pulsating blood in stenosed arteries by the Casson model.

The equation of Herschel-Bulkley in Casson fluid can be designed to one parameter equation of Newtonian consecutive equations. Chaturani and Ponalagarsamy [8] demonstrated the blood flow in the arteries, which has a cosine form of stenosis. Sriyab [16] demonstrated the blood flow across stenosis of bell and cosine form. Owasit and Sriyab [17] demonstrated the blood flow across stenosis of symmetric and asymmetric shapes by a power-law representation. Manisha et al. [13] studied the result of heat and mass transfer on blood flow having two layers in stenosed artery with porous medium. Manisha et al. [14] analyzed the power-law fluid model to find the effect of various shape stenosis. Kumar et al. [19] studied the prediction of heart diseases based on the classification model of Ensemble with Tuned Training Weights. They used an HD prediction system for the classification of heart diseases.

The Casson fluid model in stenosed arteries with cosine form stenosis was not analyzed mathematically per the existing literature survey. This present work will design a mathematical study for blood flow with a Casson model with cosine curve-shaped stenosed arteries at a low shear rate.

2. Formulation of the Problem

The blood flow is considered a steady non-Newtonian flow, and the artery is considered of cylindrical shape having cosine form stenosis. The flow is in the axial direction (z), the artery wall is considered rigid by the existence of stenosis, and the Casson model demonstrates the properties of blood. The entering and end effects are ignored because of the long length of the artery. Cylindrical polar coordinates $(r, \psi, z)$are considered to study, where *r* represents axial direction, ψ is the azimuthal angle, and *z* represents radial directions. The stenosed artery of cosine shape is represented in Fig. 1.

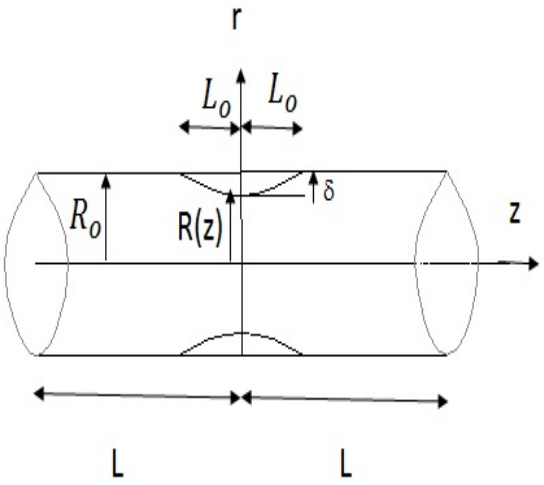

Fig. 1 Geometry of artery having stenosis.

Eq. 1 represents the governing motion equation of blood flow: -

$$\frac{-dp}{dz} = \frac{1}{r}\frac{d(r\tau)}{dr} \tag{1}$$

Shear stress is represented by τ, and *p* indicates the pressure at any point.

$$\frac{-du}{dr} = f(\tau) = \begin{cases} \frac{1}{k}\left(\sqrt{\tau} - \sqrt{\tau_c}\right)^2 & \tau \geq \tau_c \\ 0, & \tau \leq \tau_c \end{cases} \tag{2}$$

Eq. 2 represents the Casson fluid model constitutive equation. Where *k* indicates viscosity coefficient,τ_c represents yield stress, and *u* states blood velocity. The mathematical expression of the geometry of the constriction artery with cosines-form stenosis is represented by Eq. 3.

$$R(z) = R_0\left[1 - \frac{\delta}{2}\left(1 + cos\frac{\pi(z-L)}{L_0}\right)\right] \tag{3}$$

Where L represents the artery half-length, the radius of the normal and stenosed artery is denoted by R_0 and $R(z)$ respectively. δ Indicates stenosis depth at the throat. The half-length of the stenosis is represented byL_0.
Boundary conditions for the above problem can be stated as

$u = 0$ at $r = R(z)$ (4)

τ is finite at $r = 0$ (5)

3. Method of Solution

Integrating (1) and using (4), we find

$$\tau = \frac{-r}{2}\frac{dp}{dz} \tag{6}$$

From (6), the skin-friction

$$\tau_R = \frac{-R}{2}\frac{dp}{dz} \tag{7}$$

Where, $R = R(z)$

$$Q = \frac{\pi R^3}{\tau_R^3}\int_0^{\tau_R} \tau^2 f(\tau) d\tau \tag{8}$$

Q is the flow rate in Eq. 8.
Using eq. (2) in eq. (8) we have

$$Q = \frac{\pi R^3}{\tau_R^3}\int_{\tau_c}^{\tau_R} \tau^2 \frac{1}{k}\left(\sqrt{\tau} - \sqrt{\tau_c}\right)^2 d\tau \tag{9}$$

Integrating eq. (9) and after simplifying, we obtain

$$Q = \frac{\pi R^3}{4k}\tau_R\left\{1 - \frac{16}{7}\left(\frac{\tau_c}{\tau_R}\right)^{\frac{1}{2}} + \frac{4}{3}\left(\frac{\tau_c}{\tau_R}\right) - \frac{1}{21}\left(\frac{\tau_c}{\tau_R}\right)^4\right\} \tag{10}$$

Since $\frac{\tau_c}{\tau_R} \leq 1$, neglect the term$\left(\frac{\tau_c}{\tau_R}\right)^4$ in eq. (10), we obtain the flow rate as

$$Q = \frac{\pi R^3}{4k}\tau_R\left\{1 - \frac{16}{7}\left(\frac{\tau_c}{\tau_R}\right)^{\frac{1}{2}} + \frac{4}{3}\left(\frac{\tau_c}{\tau_R}\right)\right\} \tag{11}$$

Using eq. (6) in eq. (11)

$$\frac{-dp}{dz} = \frac{128\tau_c}{49R} + \frac{8}{R}\left(\frac{Qk}{\pi R^3} - \frac{\tau_c^2}{147}\right) + \frac{64}{7R}\sqrt{\frac{kQ\tau_c}{\pi R^3} - \frac{\tau_c^2}{147}} \tag{12}$$

Neglecting the term involvedτ_c^2 in eq. (12), we obtain

$$\frac{-dp}{dz} = \frac{128\tau_c}{49R} + \frac{8Qk}{\pi R^4} + \frac{64}{7R}\sqrt{\frac{kQ\tau_c}{\pi R^3}} \tag{13}$$

$p = p_1$ at $z = -L$ and $p = p_2$ at $z = L$.

$$p_1 - p_2 = \frac{128\tau_c}{49R_0}\int_{-L}^{L}\frac{dz}{\left(\frac{R}{R_0}\right)} + \frac{8Qk}{\pi R_0^4}\int_{-L}^{L}\frac{dz}{\left(\frac{R}{R_0}\right)^4} + \frac{64}{7}\sqrt{\frac{kQ\tau_c}{\pi R_0^5}}\int_{-L}^{L}\frac{dz}{\left(\frac{R}{R_0}\right)^{\frac{5}{2}}} \tag{14}$$

After simplifying eq. (14), we get

$$p_1 - p_2 = \frac{256}{49}\frac{\tau_c}{R_0}\left((L-L_0) + \int_0^{L_0}\frac{dz}{\left(\frac{R}{R_0}\right)}\right) + \frac{16Qk}{\pi R_0^4}\left((L-L_0) + \int_0^{L_0}\frac{dz}{\left(\frac{R}{R_0}\right)^4}\right) + \frac{128}{7}\sqrt{\frac{Qk\tau_c}{\pi R_0^5}}\left((L-L_0) + \int_0^{L_0}\frac{dz}{\left(\frac{R}{R_0}\right)^{\frac{5}{2}}}\right) \tag{15}$$

λ is the resistance to flow in Eq. 16.

$$\lambda = \frac{p_1 - p_2}{Q} \tag{16}$$

$$\lambda = \frac{256}{49Q}\frac{\tau_c}{R_0}\left((L-L_0) + \int_0^{L_0}\frac{dz}{\left(\frac{R}{R_0}\right)}\right) + \frac{16k}{\pi R_0^4}\left((L-L_0) + \int_0^{L_0}\frac{dz}{\left(\frac{R}{R_0}\right)^4}\right) + \frac{128}{7}\sqrt{\frac{k\tau_c}{\pi Q R_0^5}}\left((L-L_0) + \int_0^{L_0}\frac{dz}{\left(\frac{R}{R_0}\right)^{\frac{5}{2}}}\right) \tag{17}$$

The resistance to flow is denoted λ_N in the normal artery when stenosis is not present in the artery.

$$\lambda_N = \frac{16L}{R_0}\left(\frac{k}{\pi R_0^3} + \frac{16\tau_c}{49Q} + \frac{8}{7}\sqrt{\frac{k\tau_c}{\pi Q R_0^3}}\right) \tag{18}$$

The expression for a dimensionless form of resistance to flow is found as follows

$$\bar{\lambda}_1 = \frac{\lambda}{\lambda_N} = 1 - \frac{L_0}{L} + \frac{1}{L}\left(\frac{\left(\frac{16\tau_c}{49Q}\right)I_1 + \left(\frac{k}{\pi R_0^3}\right)I_2 + \frac{8}{7}\sqrt{\frac{k\tau_c}{\pi Q R_0^3}}I_3}{\frac{16\tau_c}{49Q} + \frac{k}{\pi R_0^3} + \frac{8}{7}\sqrt{\frac{k\tau_c}{\pi Q R_0^3}}}\right) \tag{19}$$

Where, $I_1 = \int_0^{L_0}\frac{dz}{\left(\frac{R}{R_0}\right)}$, $I_2 = \int_0^{L_0}\frac{dz}{\left(\frac{R}{R_0}\right)^4}$ and $I_3 = \int_0^{L_0}\frac{dz}{\left(\frac{R}{R_0}\right)^{\frac{5}{2}}}$

The resistance in the stenosed artery concerning the normal artery is denoted by $\bar{\lambda}_1$. The expression for I_1, I_2 and I_3 can be represented as: -

$$I_1 = \int_0^{L_0}\frac{dz}{\left[1 - \frac{\delta}{2}\left(1 + \cos\frac{\pi(z-L)}{L_0}\right)\right]}$$

$$I_2 = \int_0^{L_0}\frac{dz}{\left[1 - \frac{\delta}{2}\left(1 + cos\frac{\pi(z-L)}{L_0}\right)\right]^4}$$

$$I_3 = \int_0^{L_0}\frac{dz}{\left[1 - \frac{\delta}{2}\left(1 + cos\frac{\pi(z-L)}{L_0}\right)\right]^{\frac{5}{2}}} \tag{20}$$

The integrals in eq. (20) are solved by applying the two-point Gauss quadrature formula we obtained,

$$I_1 = \frac{L_0}{2\left(1 - \frac{\delta}{2}\left[1 + cos\left(\frac{\pi(-1+\sqrt{3})}{2\sqrt{3}} - \frac{L}{L_0}\right)\right]\right)} + \frac{L_0}{2\left(1 - \frac{\delta}{2}\left[1 + cos\left(\frac{\pi(1+\sqrt{3})}{2\sqrt{3}} - \frac{L}{L_0}\right)\right]\right)}$$

$$I_2 = \frac{L_0}{2\left(1-\frac{\delta}{2}\left[1+cos\left(\frac{\pi\left(-1+\sqrt{3}\right)}{2\sqrt{3}}-\frac{L}{L_0}\right)\right]\right)^4} + \frac{L_0}{2\left(1-\frac{\delta}{2}\left[1+cos\left(\frac{\pi\left(1+\sqrt{3}\right)}{2\sqrt{3}}-\frac{L}{L_0}\right)\right]\right)^4}$$

$$I_3 = \frac{\frac{L_0}{2\left(1-\frac{\delta}{2}\left[1+cos\left(\frac{\pi\left(-1+\sqrt{3}\right)}{2\sqrt{3}}-\frac{L}{L_0}\right)\right]\right)^{\frac{5}{2}}}}{} + \frac{\frac{L_0}{2\left(1-\frac{\delta}{2}\left[1+cos\left(\frac{\pi\left(1+\sqrt{3}\right)}{2\sqrt{3}}-\frac{L}{L_0}\right)\right]\right)^{\frac{5}{2}}}}{} \tag{21}$$

The non-dimensional flow resistance of non-Newtonian behaviour is derived as follows: -

$$\bar{\lambda}_2 = \frac{\text{resitance to flow of the non Newtonian fluid}}{\text{resitance to flow of the Newtonian fluid in the same stenosed artery}}$$

$$\bar{\lambda}_2 = \left[\frac{16}{49}\left(\frac{\pi\tau_c R_0^3}{Qk}\right) + 1 + \frac{8}{7}\sqrt{\frac{\pi\tau_c R_0^3}{Qk}}\right]\cdot\left(1-\frac{L}{L_0}\right) + \frac{1}{L}\left[\frac{16}{49}\left(\frac{\pi\tau_c R_0^3}{Qk}\right)I_1 + I_2 + \frac{8}{7}\sqrt{\frac{\pi\tau_c R_0^3}{Qk}}I_3\right] \tag{22}$$

$$\text{Where, } \lambda_{Ne} = \frac{16kL}{\pi R_0^4} \tag{23}$$

Which is found from eq. (17), by
$\delta = 0, R(z) = R_0$ and $\tau_c = 0$.

The derivation of skin friction is derived from eq. (7) and eq. (13),

$$\tau_R = \frac{-R}{2}\frac{dp}{dz} = \frac{R}{2}\left[\frac{128\tau_c}{49R} + \frac{8Qk}{\pi R^4} + \frac{64}{7R}\sqrt{\frac{kQ\tau_c}{\pi R^3}}\right]$$

$$\tau_R = \frac{64\tau_c}{49} + \frac{42k}{\pi R^3} + \frac{32}{7}\sqrt{\frac{kQ\tau_c}{\pi R^3}} \tag{24}$$

When $R(z) = R_0$, the skin friction is:-

$$\tau_N = \frac{64\tau_c}{49} + \frac{4Qk}{\pi R_0^3} + \frac{32}{7}\sqrt{\frac{kQ\tau_c}{\pi R_0^3}} \tag{25}$$

Skin friction in non-dimensional form is defined as the skin friction in the stenosed artery concerning its value in the normal artery. From eq. (24) and eq. (25), the dimensionless skin friction is obtained as:-

$$\bar{\tau}_1 = \frac{\tau_R}{\tau_N} = \frac{4Qk + \left(\frac{32}{7}\right)\left(Qk\tau_c\pi R_0^3\right)^{\frac{1}{2}}\left(\frac{R}{R_0}\right)^{\frac{3}{2}} + \left(\frac{64}{49}\right)\tau_c\pi R_0^3\left(\frac{R}{R_0}\right)^3}{\left(\frac{R}{R_0}\right)^3\left[4Qk + \left(\frac{32}{7}\right)\left(Qk\tau_c\pi R_0^3\right)^{\frac{1}{2}} + \left(\frac{64}{49}\right)\tau_c\pi R_0^3\right]} \tag{26}$$

The dimensionless skin friction for non-Newtonian behaviour of blood is derived as: -

$$\overline{\tau_2} = \frac{\tau_R}{\tau_{Ne}} = \frac{1}{\left(\frac{R}{R_0}\right)^3} + \frac{16}{49}\left(\frac{\pi R_0^3\tau_c}{Qk}\right) \quad + \frac{8}{7}\left(\frac{1}{\left(\frac{R}{R_0}\right)^{\frac{3}{2}}}\right)\sqrt{\frac{\pi R_0^3\tau_c}{Qk}} \tag{27}$$

$$\text{Where} \tau_{Ne} = \frac{4kQ}{\pi R_0^3} \tag{28}$$

4. Results and Analysis

The analytical expressions from equations (19), (22), (26), and (27) have been executed in MATLAB to show the results graphically. The effect of different flow properties on the flow resistance, flow rate, and skin friction are examined for different k, Q, and L values R_0. In this work, the range of these parameters has been considered as k=2.0-7.0, τ_c=0.0-0.5dyne/cm^2, Q=0-1, L=5cm, and R_0=0.40 to get data for plotting the graphs.

Fig. 2 to 6 represents the stenosis effects on flow resistance normalized with non-Newtonian fluid. A comparison of the non-dimensional flow resistance $\overline{\lambda}_1$ of cosine shape stenosis and bell shape stenosis for different models has been represented in Fig. 2. It is analyzed that resistance to flow for cosine form is more than bell form for a different kind of model. However, resistance to flow is enhanced along stenosis depth for both bell and cosine forms for different fluid types.

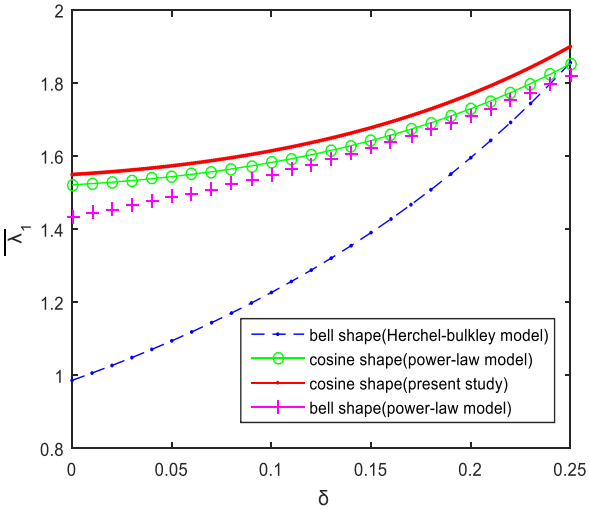

Fig. 2 Graph of dimensionless resistance to flow $\overline{\lambda}_1$ versus stenosis depth δ for various shapes.

The profile of flow resistance normalized with non-Newtonian fluid $\overline{\lambda}_1$ along the depth of stenosis δ for the various magnitude of L_0/L and k=7, Q=0.4, τ_c=0.01 is displayed in **Fig. 3**. The flow resistance increases with the enhancement of the magnitude of stenosis length L_0/L , and it has also been observed that flow resistance increases along the stenosis depth. The results of flow resistance along stenosis depth in the stenotic region are similar to the results obtained by Misra and Shit [11], contrary to the results of Sriyab [16].

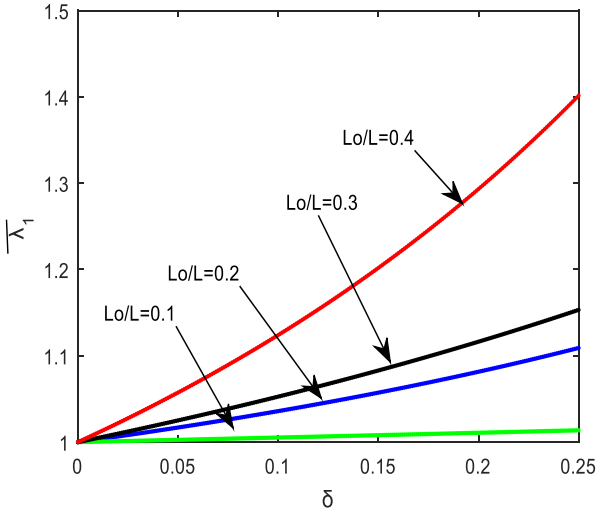

Fig. 3 Graph of flow resistance $\overline{\lambda}_1$ versus depth of stenosis δ for the different magnitude of L_0/L (k=7, Q=0.4, τ_c=0.0)

The deviation in resistance to flow normalized with non-Newtonian fluid $\overline{\lambda}_1$ at the different magnitudes of yield stress τ_c along stenosis depth δ is shown in Fig. 4. It is illustrated in Fig. 4 that resistance to flow enhances when the magnitude of yield stress reduces and it enhanced along stenosis depth.

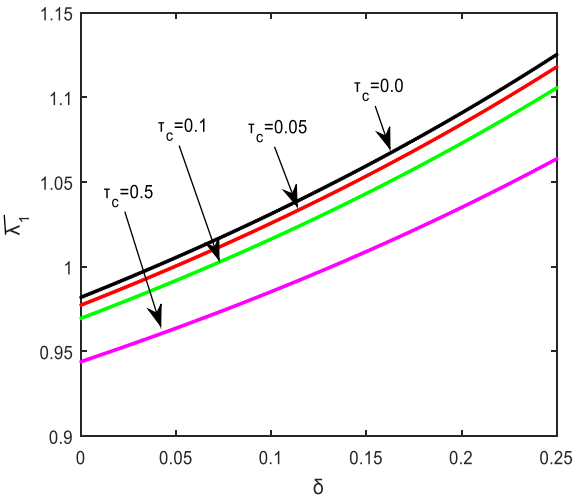

Fig. 4 Graph of resistance to flow $\overline{\lambda}_1$ versus stenosis depth δ at yield stress τ_c and k=4, Q=0.2, L_0/L=0.4).

Fig. 5 represents the resistance profile to flow normalized with Newtonian fluid $\overline{\lambda}_2$ along stenosis depth δ, and the graph is plotted for various values of stenosis length L_0/L and k=7, Q=0.4, τ_c=0. The flow resistance increases across stenosis depth, but its value reduces for the different magnitude of the stenosis length. It is examined from the figure that when the magnitudes of stenosis length increase, flow resistance diminishes.

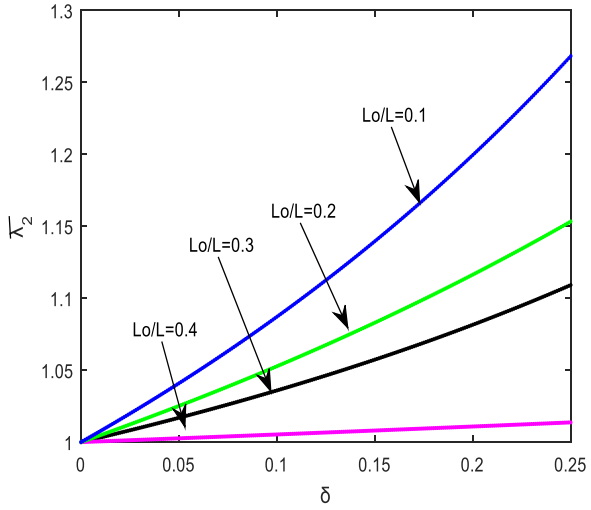

Fig. 5 Graph of resistance to flow $\bar{\lambda}_2$ versus stenosis depth δ at stenosis length L_0/L (k=7, Q=0.4, τ_c=0.0)

The deviation in resistance to flow Normalised with Newtonian fluid $\bar{\lambda}_2$ for the various magnitude of yield stress τ_c along stenosis depth δ is represented by Fig. 6. It is examined from the figure that its value increases when the magnitude of yield stress is enhanced. It is also enhanced along stenosis depth. The outcome for resistance to flow normalized with Newtonian fluid is similar to the results of Misra and Shit [11] but the opposite of Sriyab [16]. It can be investigated from fig. 2 to 6 that the effect of resistance to flow normalized with Newtonian fluid and normalized with non-Newtonian fluid exhibit different behaviour.

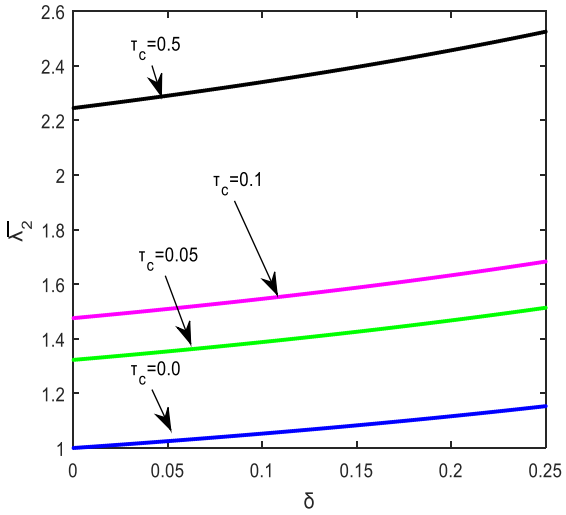

Fig. 6 Graph of resistance to flow $\bar{\lambda}_2$ versus stenosis depth δ for the different magnitude of yield stress τ_c (k=4, Q=0.2, L_0/L=0.4)

A comparison of resistance to flow normalized with the non-Newtonian fluid $\bar{\lambda}_1$ of cosine form and bell shape stenosis having Casson fluid with different types of arteries for the various value of radii and with different parameters a, δ, L_0 and m have been demonstrated in Table 1. It is evident from Table 1 that the flow resistance for cosine form stenosis increases greatly when the length of stenosis and stenosis height increase, and it increases inconsiderably for different values of radii. The resistance to the flow of bell shape stenosis is also increasing with the increase of stenosis length, and it considerably magnifies with the increase of stenosis height. But it slightly diminishes with the enhancement of stenosis length parameter m. The estimated value of resistance to flow for cosine form is moderately greater than that of bell shape stenosis. However, resistance to flow considerably increases for both shapes of stenosis for different parameter values. The comparison of the estimated value of skin friction $\bar{\tau}_2$ for cosine shape stenosis (present study) and bell shape stenosis with different magnitudes of coefficient of viscosity k, yield stress $\tau_c = 0.05$, and axial variable z has been shown in Table 2. The skin friction normalized with Newtonian fluid is higher for bell shape than cosine shape for different values of viscosity coefficient. It is also examined that skin friction reduces moderately for both bell and cosine shapes when the magnitude of viscosity coefficient k enhances.

Table 1. Estimates in resistance to flow $\bar{\lambda}_1$ for different arteries with variation in radii and $\tau_c = 0.05$δ is the stenosis depth.

Blood vessel Radius R_o(cm) Flow rate Q ($cm^3 s^{-1}$)	Cosine shape stenosis ($\bar{\lambda}_1$)		Bell shape stenosis($\bar{\lambda}_1$)				
	a=0.1 L_0=1.0	a=0.2 L_0=1.5	a=0.1 m=2 L_0=1.0	a=0.1 m=2 L_0=1.5	a=0.2 m=3 L_0=1.5	a=0.1 m=3 L_0=1.5	a=0.2 m=2 L_0=1.5
Aorta (1.71.67)	1.411	3.011	1.116	1.422	3.506	1.431	2.768
Femoral (0.3,19.63)	1.462	3.028	1.240	1.495	3.854	1.672	2.798
Carotid (0.2.12.57)	1.464	3.032	1.309	1.516	3.864	1.684	2.809
Coronary (0.05,3.47)	1.468	3.050	1.329	1.536	3.879	1.732	2.829
Arteriole (0.002,0.00002)	1.463	3.029	1.240	1.495	3.854	1.673	2.799

Table 2. Variation in skin friction $\bar{\tau}_2$ for the different magnitude of viscosity coefficient k at yield stress $\tau_c = 0.05$ and with L_0/L=0.5.

z	$\bar{\tau}_2$(present study)			$\bar{\tau}_2$ (bell shape stenosis)		
	k=2	k=4	k=7	k=2	k=4	k=7
-1.5	1.395	1.311	1.263	1.755	1.651	1.591
-1	1.857	1.747	1.684	2.445	2.303	2.220
-0.5	2.550	2.402	2.316	3.525	3.323	3.204
0	2.940	2.771	2.672	4.181	3.942	3.802
0.5	2.550	2.402	2.316	3.525	30323	3.204
1	1.857	1.747	1.684	2.445	2.303	2.220
1.5	1.395	1.311	1.263	1.755	1.651	1.591

A comparison of dimensionless skin friction $\bar{\tau}_2$ for various models has been demonstrated in Figure 7. It is analyzed from the figure that skin friction in bell form stenosis is higher than in cosine form (for any type of fluid). However, skin friction normalized with Newtonian fluid increases for both bell and cosine shapes from the artery entry point to the mid-point, decreasing from the artery mid-point to the exit point.

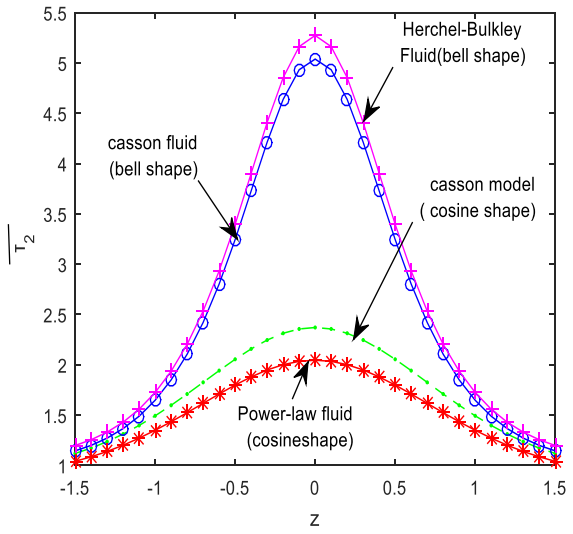

Fig. 7 comparison of normalized skin friction $\bar{\tau}_2$ along z for various fluids.

Fig. 8 represents the profile of skin friction normalized with non-Newtonian fluid versus stenosis depth δ at the various magnitude of yield stress τ_c (k=4, Q=0.4, =0.3). It can be observed from the figure that normalized skin friction of the stenotic region reduces inconsiderably as the magnitude of yield stress enhances. It is also detected that normalized skin friction increases along stenosis depth. Fig. 9 shows the graph of skin friction normalized with non-Newtonian fluid $\bar{\tau}_1$ versus axial distance for the magnitudes of τ_c and L_0/L. The skin friction has the least value at the edges of the stenosis; however, it has the maximum value at the throat of stenosis. Furthermore, it is also illustrated from Fig.9 that skin friction normalized with non-Newtonian fluid enhances when the magnitude of stenosis length increases for a fixed magnitude of yield stress. Furthermore, it is also examined that skin friction reduces when the magnitude of yield stress diminishes for a fixed magnitude of stenosis length.

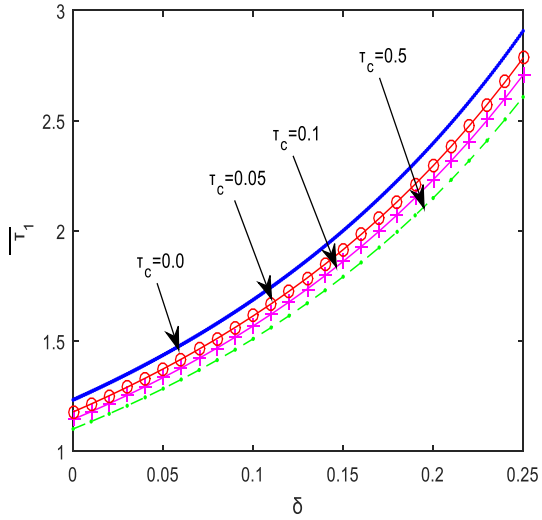

Fig. 8 Graph skin friction $\bar{\tau}_1$ versus stenosis depth δ at various yield stress τ_c (k=4, Q=0.4, L_0/L=0.3).

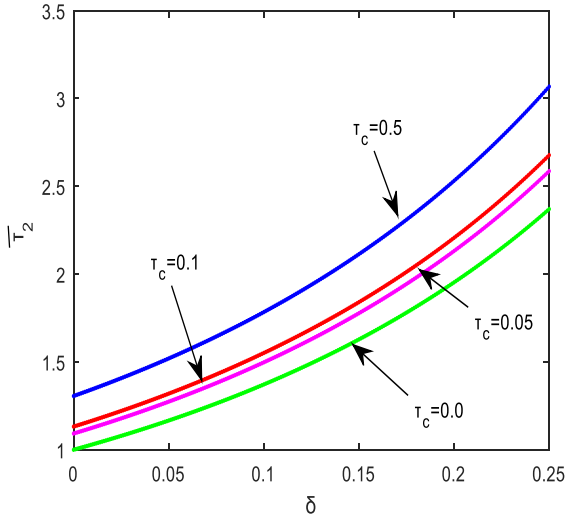

Fig. 10 variation in skin friction $\bar{\tau}_2$ with stenosis depth δ for various yield stress τ_c (k=4, Q=0.4).

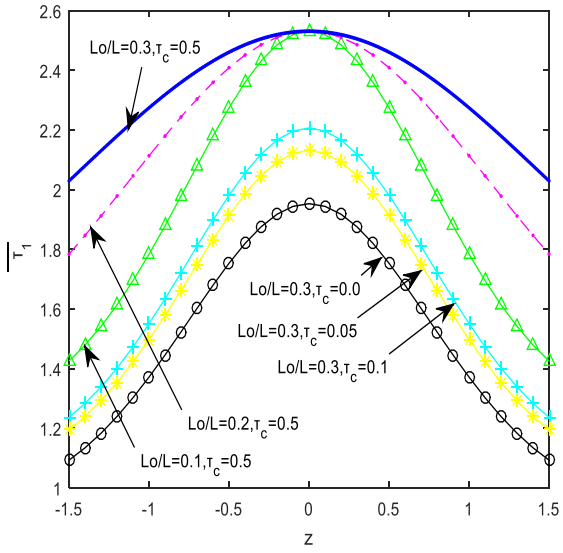

Fig. 9 Graph skin friction $\bar{\tau}_1$ versus axial distance at various yield stress τ_c and stenosis length L_0/L(k=4, Q=0.4).

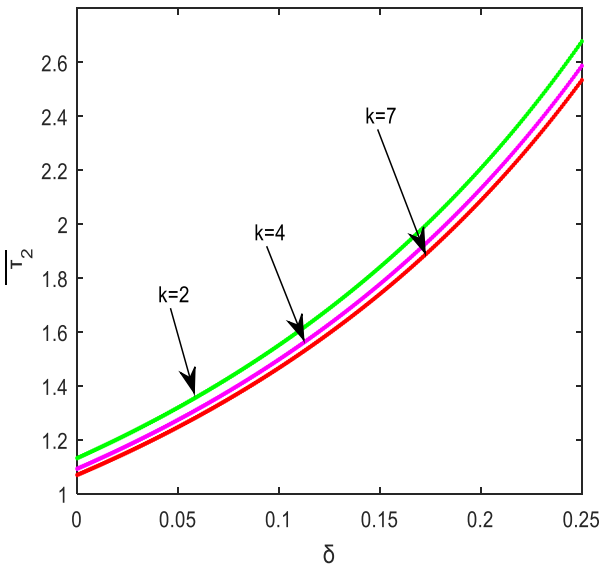

Fig. 11 Graph of skin friction $\bar{\tau}_2$ versus depth of stenosis δ for the different magnitudes of the coefficient of viscosity k (τ_c=0.05, Q=0.4).

The profile of skin friction normalized with Newtonian fluid $\bar{\tau}_2$ with the stenosis depth is represented in Fig. 10. The skin friction is enhanced slightly as the magnitude of yield stress is enhanced, and it is also detected that the skin friction is enhanced along stenosis depth. The variation in the profile of skin friction $\bar{\tau}_2$ along the stenosis depth at the different magnitude of viscosity coefficient is represented in Fig. 11. The skin friction reduces when the viscosity coefficient k increases, and the skin friction enhances along stenosis depth.

The variation of skin friction normalized with Newtonian fluid $\bar{\tau}_2$ along axial distance z for the different magnitude of yield stress and viscosity coefficient has been represented by Fig. 12 and Fig. 13. It is examined from figures that the skin friction enhances from the artery entry point to the mid-point of the artery. It reduces from the mid-point to the outlet of the artery. A comparison between Fig.12 and Fig.13 shows that skin friction is varied slightly by the magnitude of yield stress, and the skin friction is highly affected by the magnitude of the viscosity coefficient. The result is similar to the results of Misra and Shit [11].

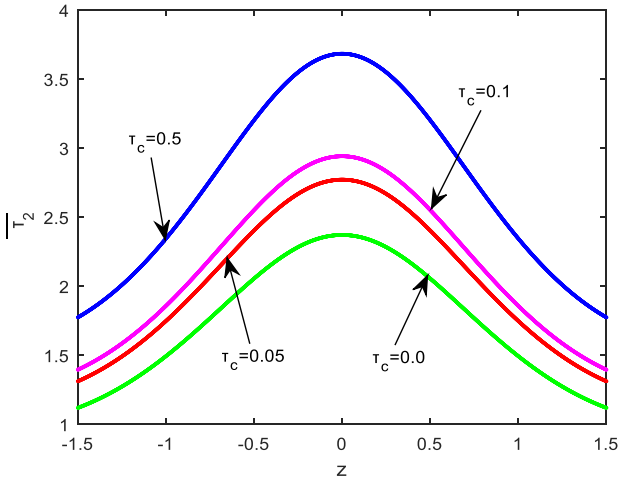

Fig. 12 variation in skin friction $\bar{\tau}_2$ at an axial distance for various yield stress τ_c (k= 4, Q=0.4).

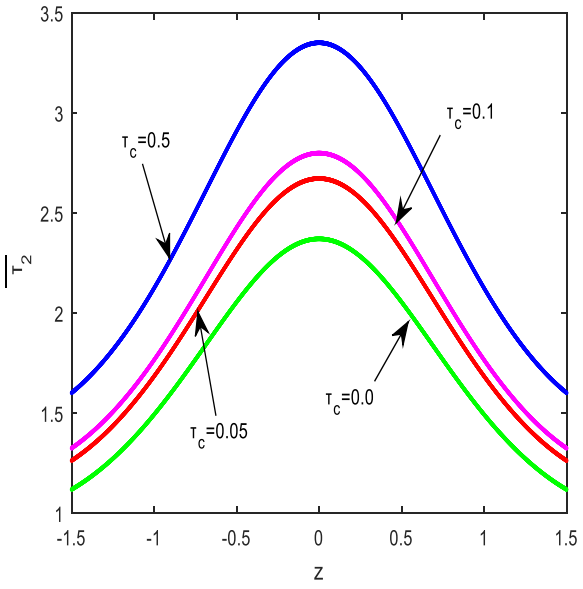

Fig. 13 variation in skin friction $\bar{\tau}_2$ at an axial distance for various magnitudes of yield stress τ_c (k= 2, Q=0.4).

The comparison of flow rate along axial distance for various types of fluid has been represented in Fig. 14. It is revealed from the figure that the flow rate for the cosine shape is higher than for the bell shape. Furthermore, it is found that the flow rate curve for bell shape with the Casson model lies between the plots of bell form with Herschel-Bulkley fluid and cosine form of Power-law fluid.

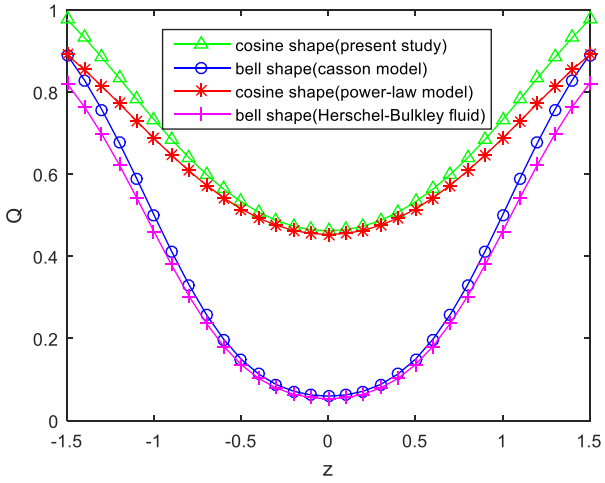

Fig. 14 Graph flow rate Q versus axial distance for various types of the fluid model.

Fig. 15 shows the plot of flow rate Q versus z at the various magnitude of the coefficient of viscosity k and yield stress τ_c. The flow rate decreases with either the viscosity coefficient or yield stress. The flow rate is highest at the edges of the stenosed artery and lowest at the stenosis throat.

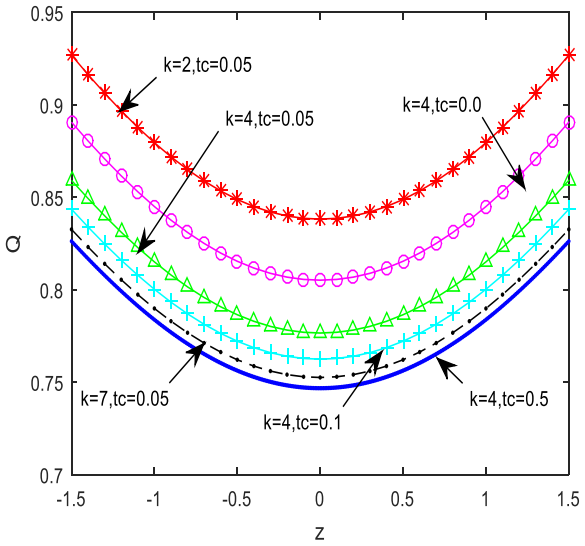

Fig. 15 Graph flow rate versus z at the different magnitudes of yield stress τ_c and viscosity coefficient k.

The variation in flow rate for the different magnitude of stenosis length along axial direction has been shown in Fig.16. It is observed from the figure that flow rate decreases when the length of stenosis increases and flow rate is minimum at the neck of the artery. It achieves maximum at the edge of the artery.

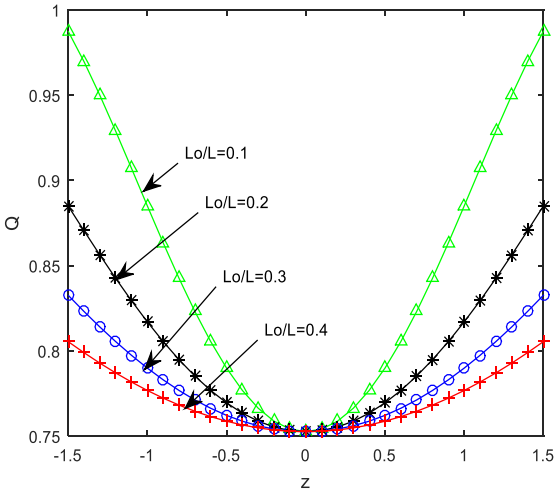

Fig. 16 Graph flow rate versus z at the different magnitudes of stenosis length and k=4.

5. Conclusion

A mathematical analysis of a non-Newtonian blood flow model with cosine-shaped stenosis in the artery is presented by considering blood as Casson fluid. The outcomes of this work have been compared with the outcomes of Misra and Shit for bell shape (Herchel-Bulkley fluid) [11] and Sriyab for cosine and bell shape (Power-law fluid) [16]. The main observations are as follows:

1. Skin friction for bell shape for a different type of fluid is higher than cosine shape. It can be detected that the bell shape greatly impacts skin friction (friction against the artery membrane) more than the cosine shape.
2. Flow resistance for cosine form for a different fluid type is higher than bell shape. This implies that resistance to flow for cosine shape stenosis greatly impacts blood to flow more than bell shape stenosis.
3. Resistance to flow for normalized with Newtonian fluid and normalized with non-Newtonian fluid (i.e. the effect of stenosis and non-Newtonian fluid) different exhibit behaviour.
4. Flow rate for cosine shape stenosis is higher than bell shape stenosis in the stenotic region. It can be determined that cosine shape stenosis with Casson fluid greatly influences flow rate more than bell shape stenosis with Casson fluid.

Therefore, it is investigated that different geometry of stenosis like cosine and bell shape stenosis, length, yield stress, viscosity coefficient, and depth of stenosis are the important aspects that affect the blood flow in the stenosed artery. Further, the study of non-Newtonian blood flow with various models could be an important step in curing and diagnosing cardiovascular diseases.

References

[1] Aroesty J & Gross J.F, "Pulsatile Flow in the Small Blood Vessel," *I. Casson Theory, Biorheology*, vol. 9, no. 1, pp. 33-43, 1972.

[2] Blair G.W.S, "An Equation for the Flow of Blood, Plasma and Serum through Glass Capillaries," *Nature*, vol. 183, no. 4661, pp. 613-614, 1959.

[3] Blair G.W.S. & Spanner D.C, "*An Introduction to Biorheology*," Elsevier Scientific, Oxford, UK, 1974.

[4] Casson N, "*Rheology of Disperse Systems in Flow Equation for Pigment Oil Suspensions of the Printing Ink Type*," Rheology of Disperse System, Pergamon Press, London, UK, pp. 84-102, 1959.

[5] Copley A.L, "*Apparent Viscosity and Wall Adherence of Blood Systems in Flow Properties of Blood and Other Biological Systems*," Pergamon Press, Oxford, UK, pp. 84-102, 1960.

[6] Charm S, & Kurland G, "Viscometry of Human Blood for Shear Rates of 0-100,000 〖sec〗^(-1)," *Nature*, vol. 206, no. 4984, pp. 617-618, 1965.

[7] Chaturani P, & Samy R.P, "Pulsatile Flow of Casson's Fluid through Stenosed Arteries with Application to Blood Flow," *Biorheology*, vol. 23, no. 5, pp. 499-511, 1986.

[8] Chaturani P, & Ponnalagar Samy V. R, "A Study of Non-Newtonian Aspects of Blood Flow through Stenosed Arteries and its Applications in Arterial Diseases," *Biorheology*, vol. 22, no. 6, pp. 521-531, 1985.

[9] Deshpande M.D, Giddens D.P & Mabon R.F, "Steady Laminar Flow through Modelled Vascular Stenosis," *Journal of Biomechanics*, vol. 9, no. 4, pp. 165-174, 1976.

[10] Lorenzini G & Casalena E, "CFD Analysis of Pulsatile Blood Flow in a Human Atherosclerotic Artery with Eccentric Plaques," *Journal of Biomechanics*, vol. 41, no. 9, pp. 1862-1870, 2008.

[11] Misra J.C & Shit G.C, "Blood Flow through Arteries in a Pathological State: A Theoretical Study," *International Journal of Engineering Science*, vol. 44, no. 10, pp. 662-671, 2006.

[12] Merrill E.W, Benis A.M, Gilliland E.R, Sherwood T.K, and Salzman W, "Pressure Flow Relations of Human Blood in Hollow Fibres at Low Flow Rates," *Journal of Applied Physiology*, vol. 20, no. 5, pp. 954-967, 1965.

[13] Manisha, Nasha V & Kumar S, "MHD Two-layered Blood Flow Under the Effect of Heat and Mass Transfer in Stenosed Artery with Porous Medium," *International Journal of Advanced Research in Engineering and Technology*, vol. 12, no. 6, pp. 63-76, 2021.

[14] Manisha, Nasha V & Kumar S, "Non-Newtonian Blood Flow Model with the Effect of Different Geometry of Stenosis," *Journa1 of Mathematical and Computational Sciences*, vol. 12, pp. 1-21, 2022.

[15] Shukla J.B, Parihar R.S & Rao B.R.P, "Effects of Stenosis on the Non-Newtonian Flow of the Blood in an Artery," *Bulletin of Mathematical Biology*, vol. 42, no. 3, pp. 283-294, 1980.

[16] Sriyab S, "The Effect of Stenotic Geometry and Non-Newtonian Property of Blood Flow through Arterial Stenosis," *Bentham Science*, vol. 20, pp. 16-30, 2020.

[17] Owasit P & Sriyab S, "Mathematical Modelling of Non-Newtonian Fluid in Arterial Blood Flow through Various Stenosis," *Advances in Difference Equations*, vol. 20, 2021.

[18] Young D.F, "Effect of Time-Dependent Stenosis on Flow through a Tube," *Journal of Manufacturing Science and Engineering*, vol. 90, no. 2, pp. 248-254, 1968.

[19] Kumar P. R, Ravichandran & S, Narayana S, "Heart Disease Prediction based on Ensemble Classification Model with Tuned Training Weights," *International Journal of Engineering Trends and Technology*, vol. 70, no. 4, pp. 59-81, 2022.